Inorganic Chemistry

Article

pubs.acs.org/IC

Characterization and Dioxygen Reactivity of a New Series of Coordinatively Unsaturated Thiolate-Ligated Manganese(II) Complexes

Michael K. Coggins, Santiago Toledo, Erika Shaffer, Werner Kaminsky,[†] Jason Shearer,[‡] and Julie A. Kovacs*

The Department of Chemistry, University of Washington, Campus Box 351700, Seattle, Washington 98195-1700, United States

Supporting Information

ABSTRACT: The synthesis, structural, and spectroscopic characterization of four new coordinatively unsaturated mononuclear thiolate-ligated manganese(II) complexes ([$Mn^{II}(S^{Me2}N_4$(6-Me-DPEN))](BF_4) (**1**), [$Mn^{II}(S^{Me2}N_4$(6-Me-DPPN))]$(BPh_4)\cdot$MeCN (**3**), [$Mn^{II}(S^{Me2}N_4$(2-QuinoPN))]$(PF_6)\cdot$MeCN$\cdot Et_2O$ (**4**), and [$Mn^{II}(S^{Me2}N_4$(6-H-DPEN)(MeOH)](BPh_4) (**5**)) is described, along with their magnetic, redox, and reactivity properties. These complexes are structurally related to recently reported [$Mn^{II}(S^{Me2}N_4$(2-QuinoEN))](PF_6) (**2**) (Coggins, M. K.; Kovacs, J. A. *J. Am. Chem. Soc.* **2011**, *133*, 12470). Dioxygen addition to complexes **1**−**5** is shown to result in the formation of five new rare examples of Mn(III) dimers containing a single, unsupported oxo bridge: [$Mn^{III}(S^{Me2}N_4$(6-Me-DPEN)]$_2$-(μ-O)$(BF_4)_2\cdot$2MeOH (**6**), [$Mn^{III}(S^{Me2}N_4$(QuinoEN)]$_2$-(μ-O)$(PF_6)_2\cdot Et_2O$ (**7**), [$Mn^{III}(S^{Me2}N_4$(6-Me-DPPN)]$_2$-(μ-O)$(BPh_4)_2$ (**8**), [$Mn^{III}(S^{Me2}N_4$(QuinoPN)]$_2$-(μ-O)$(BPh_4)_2$ (**9**), and [$Mn^{III}(S^{Me2}N_4$(6-H-DPEN)]$_2$-(μ-O)$(PF_6)_2\cdot$2MeCN (**10**). Labeling studies show that the oxo atom is derived from $^{18}O_2$. Ligand modifications, involving either the insertion of a methylene into the backbone or the placement of an ortho substituent on the N-heterocyclic amine, are shown to noticeably modulate the magnetic and reactivity properties. Fits to solid-state magnetic susceptibility data show that the Mn(III) ions of μ-oxo dimers **6**−**10** are moderately antiferromagnetically coupled, with coupling constants (2*J*) that fall within the expected range. Metastable intermediates, which ultimately convert to μ-oxo bridged **6** and **7**, are observed in low-temperature reactions between **1** and **2** and dioxygen. Complexes **3**−**5**, on the other hand, do not form observable intermediates, thus illustrating the effect that relatively minor ligand modifications have upon the stability of metastable dioxygen-derived species.

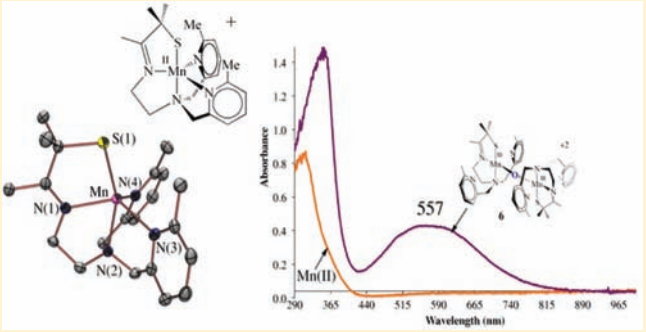

INTRODUCTION

Nature utilizes manganese ions to promote a wide variety of oxidative transformations. The active sites of these metalloenzymes, examples of which include manganese lipoxygenase (MnLO),[1−4] ribonucleotide reductases,[5] manganese superoxide dismutases (MnSOD),[6−9] catalases,[10] and the oxygen evolving complex of photosystem II,[11,12] vary in terms of Mn ion nuclearity and oxidation state. Despite these structural and electronic differences, a unifying characteristic of this broad class of metalloenzymes is that reactive Mn-superoxo, -peroxo, or -oxo intermediates are proposed to form upon reaction with dioxygen, or reduced derivatives (O_2^-, H_2O_2, H_2O) thereof. There are, however, very few well-characterized biological or synthetic examples of such species.[13−26] By exploring the dioxygen chemistry of Mn^{2+} we should be able to improve our understanding of the characteristic properties of Mn-dioxygen intermediates and their thermodynamically favored products, as well as the mechanisms by which they form.

Metastable O_2-derived intermediates have also been established to form in a variety of cysteinate-ligated metalloenzymes, including the heme-containing cytochrome P450[27,28] and nonheme superoxide reductase.[29,30] Reactivity studies involving small molecule thiolate-ligated transition-metal complexes and dioxygen, or dioxygen-derived oxidants have increased our understanding of the structural, electronic, and reactivity properties of these metastable enzyme intermediates. It has also been demonstrated that thiolate ligands help to promote the activation of strong N−O and RC≡N bonds,[31−33] as well as facilitate the reduction of dioxygen and superoxide.[34−37] Thiolate ligands have been shown to stabilize coordinatively unsaturated M(II) complexes (M = Mn, Fe, Co, Ni, Cu, Zn),[38,39] impart rich spectroscopic properties,[30] significantly lower redox potentials,[30,34] lower the activation barrier to dioxygen binding,[40] and help create potent high-valent metal-oxos capable of activating C−H bonds.[28,41]

To further our understanding of the influence that thiolate ligands have upon biologically relevant transition metals, we

Received: January 25, 2012
Published: May 29, 2012

have begun to explore the structural and reactivity properties of thiolate-ligated Mn(II) complexes. Described herein are the syntheses and X-ray crystal structures of a new series of coordinatively unsaturated mononuclear alkyl thiolate-ligated Mn(II) complexes constructed from related N-heterocyclic containing ligand frameworks. Magnetic, electronic, and redox properties are also described, as well as the properties of their corresponding oxo derivatives.

EXPERIMENTAL SECTION

General Methods. All manipulations were performed using Schlenk line techniques or under an N_2 atmosphere in a glovebox. Reagents and solvents were purchased from commercial vendors, were of the highest available purity, and were used without further purification unless otherwise noted. MeOH (Na), MeCN (CaH_2), and CH_2Cl_2 (CaH_2) were dried and distilled prior to use. Et_2O was rigorously degassed and purified using solvent purification columns housed in a custom stainless steel cabinet and dispensed by a stainless steel Schlenk-line (GlassContour). ^{1}H NMR spectra were recorded on either a Bruker AV 301 or Bruker AV 300 FT NMR spectrometer at ambient temperature and were referenced to residual deuterated solvent. Chemical shifts are listed in parts per million (ppm). UV/vis spectra were recorded on a Varian Cary 50 spectrophotometer equipped with a fiber optic cable connected to a "dip" ATR probe (C-technologies). A custom-built two-neck solution sample holder equipped with a threaded glass connector was sized specifically to fit the "dip" probe. Electrospray-ionization mass spectra were obtained on a Bruker Esquire Liquid Chromatograph-Ion Trap mass spectrometer. Electron paramagnetic resonance (EPR) spectra were recorded on a Bruker E580 CW-EPR spectrometer operating at X-band frequency between 4 and 7 K with an Oxford helium cryostat. EPR spectra were collected with the following spectrometer parameters: frequency = 9.396 GHz, power = 2.008 mW, attenuation = 20 dB, sweep width = 6,000 G, gain = 1×10^3, conversion time = 5.4 ms, time constant = 5.4 ms. Magnetic moments (solid state) were obtained with polycrystalline samples in gel-caps from 5 to 300 K by zero-field cooling experiments using a Quantum Design MPMS S5 SQUID magnetometer. Pascal's constants were used to correct for diamagnetic contributions to the experimental magnetic moment. Solution magnetic moments were calculated by Evans method, with temperature correction made in the manner described by Van Geet.[42,43] Cyclic voltammograms were recorded in MeCN (100 mM $Bu^n_4N(PF_6)$ supporting electrolyte) on a PAR 263A potentiostat utilizing a glassy carbon working electrode, platinum auxiliary electrode, and a $Ag^+/AgNO_3$ reference electrode. X-ray crystallography data was recorded on either a Bruker APEX II single crystal X-ray diffractometer with Mo-radiation or a Bruker SMART Apex CCD diffractometer with Mo Kα radiation. Elemental analyses were performed by Galbraith Atlantic Microlabs, Norcross, GA. 3-Methyl-3-mercapto-2-butanone, 1-(*tert*-butyloxycarbonyl)ethyldiamine (NNBoc), *N*,*N*-[bis(2-quinolinemethyl)]ethane-1,3-diamine (2-QuinoEN, L_2), and $[Mn^{II}(S^{Me2}N_4(2\text{-QuinoEN}))](PF_6)\cdot Et_2O$ (**2**) were prepared as previously described.[13]

Synthesis of 1-(*tert*-Butyloxycarbonyl)propyldiamine (NPNBoc). To a stirred solution of 1,3-diaminopropane (3.10 g, 41.9 mmol) in CH_2Cl_2 (25 mL), a 100 mL solution of di-*tert*-butyl dicarbonate (1.52 g, 6.9 mmol) was added via an addition funnel at room temperature over 3 h. The resulting solution was allowed to continue to stir for a total of 24 h. White insolubles were filtered, and the solution was washed with saturated Na_2CO_3 (2×100 mL), brine (2×100 mL), and finally dried over Na_2SO_4. The solvent was then removed under reduced pressure, and the title compound was afforded as a viscous clear oil in 63% (0.76 g, 4.3 mmol). ^{1}H NMR (300 MHz, $CDCl_3$): δ 3.21 (q, 2H), 2.75 (t, 2H), 1.60 (t, 2H), 1.43 (s, 9H). ESI-MS: Expected m/z for $C_8H_{18}N_2O_2$ = 174.241, found m/z = 175.3.

Synthesis of 2-(Chloromethyl)-6-methylpyridine Hydrochloride. A solution of 6-methyl-2-(hydroxymethyl)pyridine hydrochloride (5.00 g, 40.6 mmol) in CH_2Cl_2 (10 mL) was cooled in an ice water bath to 0 °C under an inert atmosphere. Thionyl chloride (24.15 g, 244.1 mmol) was slowly added to the solution over a period of 1 h. The resulting mixture was allowed to slowly warm to room temperature overnight, followed by evaporation of all volatiles to result in a pink solid. The pink solid was redissolved in warm EtOH (30 mL) and slowly layered with cool Et_2O (80 mL) to cause the rapid precipitation of the title compound as a white solid. The product was isolated via filtration and dried under vacuum overnight to result in 99% yield (7.13 g, 40.2 mmol). ^{1}H NMR (300 MHz, $CDCl_3$): δ 8.27 (t, 1H), 7.89 (d, 1H), 7.60 (d, 1H), 3.50 (s, 2H), 3.05 (s, 3H).

Synthesis of *N*-(*tert*-Butyloxycarbonyl)-*N*′,*N*′-[bis(6-methyl-2-pyridilmethyl)ethane-1,2-diamine] (6-Me-DPENBoc). NNBoc (1.20 g, 7.5 mmol) was dissolved in 5 M NaOH (15 mL) and added to a stirring solution of 2-(chloromethyl)-6-methylpyridine hydrochloride (2.27 g, 12.7 mmol) that was also dissolved in 5 M NaOH (15 mL). The solution was allowed to stir at room temperature for 4 days. Water (25 mL) was then added to the reaction mixture, followed by the extraction of crude organics with CH_2Cl_2 (3×50 mL). The combined organics were washed with brine (3×100 mL), dried over Na_2SO_4, and dried under vacuum to afford an orange residue. The residue was chromatographed on silica gel using a 92:8 acetone:MeOH eluent mixture. Concentration of all fractions containing the desired product resulted in isolation of the title compound as an orange oil in 63% yield (1.75 g, 4.7 mmol). ^{1}H NMR (300 MHz, $CDCl_3$): δ 7.51 (t, 2H), 7.21 (d, 2H), 7.00 (d, 2H), 3.81 (s, 4H), 3.20 (m, 2H), 2.68 (t, 2H), 2.55 (s, 6H), 1.44 (s, 9H). ESI-MS: Expected m/z for $C_{21}H_{30}N_4O_2$ = 370.5, found m/z = 371.5.

Synthesis of *N*,*N*-Bis(6-methyl-2-pyridilmethyl)ethane-1,2-diamine (6-Me-DPEN, L_1). 6-MeDPENBoc (5.50 g, 14.8 mmol) was dissolved in CH_2Cl_2 (10 mL) at room temperature and added to a 25 mL pear-shaped flask charged with a stirbar. Slow addition of trifluoroacetic acid (17.00 g, 149.1 mmol) to the stirring solution resulted in a brown mixture that was allowed to continue stirring overnight. Evaporation of all volatiles resulted in a viscous brown oil that was mixed with 5 M NaOH (20 mL) and extracted with CH_2Cl_2 (3×20 mL). The combined organics were washed with brine (3×50 mL) and dried over Na_2SO_4. Removal of all volatiles in vacuo afforded the title compound as a pale orange oil in 89% yield (3.57 g, 13.2 mmol). ^{1}H NMR (300 MHz, $CDCl_3$): δ 7.54 (t, 2H), 7.33 (d, 2H), 7.00 (d, 2H), 3.81 (s, 4H), 2.77 (t, 2H), 2.64 (t, 2H), 2.53 (s, 6H). ESI-MS: Expected m/z for $C_{16}H_{22}N_4$ = 270.2, found m/z = 271.3.

Synthesis of *N*-[*tert*-Butyloxycarbonyl]-*N*′-*N*′-[bis(6-methyl-2-pyridilmethyl)]propane-1,3-diamine] (6-Me-DPPNBoc). Following a similar procedure described for the preparation of 6-MeDPEN(Boc), NPNBoc (1.30 g, 7.5 mmol) was reacted with 2-(chloromethyl)-6-methylpyridine hydrochloride (2.40 g, 13.5 mmol) to afford a crude product that was chromatographed on silica gel using a 94:6 acetone/MeOH eluent mixture. The title compound was obtained as an orange oil in 66% yield (1.89 g, 4.9 mmol). ^{1}H NMR (300 MHz, $CDCl_3$): δ 7.52 (t, 2H), 7.30 (d, 2H), 7.00 (d, 2H), 3.74 (s, 4H), 3.13 (m, 2H), 2.58 (t, 2H), 2.53 (s, 6H), 1.67 (q, 2H), 1.41 (s, 9H). ESI-MS: Expected m/z for $C_{22}H_{32}N_4O_2$ = 384.5, found m/z = 385.6.

Synthesis of *N*,*N*-Bis(6-methyl-2-pyridilmethyl)propane-1,3-diamine (6-Me-DPPN, L_3). Following a similar procedure used for the preparation of 6-MeDPEN, 6-MeDPPNBoc (5.20 g, 13.5 mmol) was reacted with trifluoroacetic acid (17.00 g, 149.1 mmol) to afford the title compound as a pale orange oil in 88% yield (3.38 g, 11.9 mmol). ^{1}H NMR (300 MHz, $CDCl_3$): δ 7.54 (t, 2H), 7.35 (d, 2H), 7.00 (d, 2H), 3.77 (s, 4H), 2.71 (t, 2H), 2.59 (t, 2H), 2.52 (s, 6H), 1.69 (q, 2H). ESI-MS: Expected m/z for $C_{17}H_{24}N_4$ = 284.2, found m/z = 285.3.

Synthesis of *N*-(*tert*-Butyloxycarbonyl)-*N*′-*N*′-[bis(2-quinolinemethyl)]propane-1,3-diamine (2-QuinoPNBoc). Using the procedure outlined in the preparation of 6-Me-DPENBoc, NPNBoc (1.20 g, 6.9 mmol) was reacted with 2-(chloromethyl)-quinoline hydrochloride (2.70 g, 12.7 mmol) resulting in a crude oil that was chromatographed on silica gel using a 92:8 acetone/MeOH eluent mixture. The title compound was obtained as a dark orange solid in 64% yield (2.19 g, 4.8 mmol). ^{1}H NMR (300 MHz, $CDCl_3$): δ 8.09 (d, 4H), 7.76 (d, 2H), 7.66 (m, 4H), 7.48 (t, 2H), 5.79 (bs, 1H),

dx.doi.org/10.1021/ic300192q | Inorg. Chem. 2012, 51, 6633−6644

3.98 (s, 4H), 3.18 (m, 2H), 2.70 (t, 2H), 1.74 (m, 2H), 1.37 (s, 9H). ESI-MS: Expected m/z for $C_{28}H_{32}N_4O_2$ = 456.6, found m/z = 457.6.

Synthesis of *N,N*-[Bis(2-quinolinemethyl)]propane-1,3-diamine (2-QuinoPN, L_4). Following the procedure outlined in the preparation of 6-MeDPEN, 2-QuinoPNBoc (2.10 g, 4.6 mmol) was reacted with trifluoroacetic acid (17.00 g, 149.1 mmol) to afford the title compound as a pale orange solid in 91% yield (1.63 g, 4.6 mmol). ^{1}H NMR (300 MHz, $CDCl_3$): δ 8.14 (d, 2H), 8.06 (d, 2H), 7.78 (d, 2H), 7.71 (d, 2H), 7.68 (m, 2H), 4.01 (s, 4H), 2.70 (m, 4H), 1.72 (q, 2H). ESI-MS: Expected m/z for $C_{23}H_{24}N_4$ = 356.5, found m/z = 357.5.

Synthesis of *N*-(*tert*-Butyloxycarbonyl)-*N′,N′*-[bis(2-pyridilmethyl)ethane-1,2-diamine] (6-H-DPENBoc). Using the procedure outlined in the preparation of 6-Me-DPENBoc, NNBoc (1.20 g, 7.5 mmol) was reacted with 2-picolyl chloride hydrochloride (2.70 g, 12.7 mmol) resulting in a crude oil that was chromatographed on silica gel using a 95:5 acetone/MeOH eluent mixture. The title compound was obtained as a dark orange solid in 65% yield (1.67 g, 4.9 mmol). ^{1}H NMR (300 MHz, $CDCl_3$): δ 8.54 (d, 2H), 7.63 (t, 2H), 7.41 (d, 2H), 7.14 (t, 2H), 5.79 (bs, 1H), 3.86 (s, 4H), 3.21 (m, 2H), 2.70 (t, 2H), 1.44 (s, 9H). ESI-MS: Expected m/z for $C_{19}H_{26}N_4O_2$ = 342.4, found m/z = 343.1.

Synthesis of *N,N*-Bis(2-pyridilmethyl)ethane-1,2-diamine (6-H-DPEN, L_5). Following the procedure outlined in the preparation of 6-MeDPEN, 6-H-DPENBoc (5.06 g, 14.8 mmol) was reacted with trifluoroacetic acid (16.80 g, 149 mmol) to afford the title compound as a pale orange solid in 85% yield (3.04 g, 12.6 mmol). ^{1}H NMR (300 MHz, $CDCl_3$): δ 8.45 (d, 2H), 7.56 (t, 2H), 7.40 (d, 2H), 7.06 (t, 2H), 2.71 (t, 2H), 2.58 (t, 2H). ESI-MS: Expected m/z for $C_{14}H_{18}N_4$ = 242.3, found m/z = 242.2.

Synthesis of $[Mn^{II}(S^{Me2}N_4$(6-Me-DPEN))$](BF_4)$ (1). Sodium methoxide (0.210 g, 3.9 mmol), 3-methyl-3-mercapto-2-butanone (0.460 g, 3.9 mmol), and L_1 (1.02 g, 3.8 mmol) were individually dissolved in MeOH (2 mL) and cooled for 30 min at −30 °C in a drybox. The sodium methoxide and 3-mercapto-3-methyl-2-butanone solutions were then combined, and the resulting mixture was allowed to stir at room temperature for 30 min. This solution was then slowly added to a Schlenk flask charged with manganese sulfate monohydrate (0.630 g, 3.7 mmol) and a stirbar. The methanolic solution of L_1 was then slowly added, producing a yellow mixture that was allowed to stir at room temperature overnight. Sodium tetrafluoroborate (0.41 g, 3.7 mmol) was dissolved in MeOH (2 mL) and added to the solution, which was then permitted to continue stirring at room temperature for 2 days. Removal of all volatiles in vacuo afforded a yellow solid that was redissolved in MeCN (10 mL), filtered through a fine frit, and concentrated to minimal volume (2−3 mL). The resulting solution was carefully layered with Et_2O (5 mL), and the mixture was allowed to cool at −30 °C overnight. Filtration of the mixture resulted in **1** as a pale yellow crystalline solid in 53% yield (1.02 g, 2.0 mmol). Electronic absorption spectrum: λ_{max} (nm) (ε (M^{-1} cm^{-1})) (MeCN): 317(350); (EtCN): 317(305); (MeOH): 297(477); (CH_2Cl_2): 327(350). IR (Nujol): $\nu_{C=N}$ 1605 cm^{-1}. EPR spectrum (9:1 MeOH/EtOH glass): g = 2.00. Redox potential (MeCN vs SCE, 298 K): $E_{1/2}(Mn^{III/II})$ = 410 mV. Magnetic moment (solid state, 5−300 K): 5.83 μ_B; (solution, MeOH, 301 K): 5.89 μ_B. ESI-MS: Expected m/z for $[C_{21}H_{29}N_4SMn]^+$ = 424.4, found m/z = 424.3. Elemental Analysis for $C_{21}H_{29}BN_4F_4SMn$; Calculated: C, 49.33; H, 5.72; N, 10.96. Found: C, 48.36; H, 5.58; N, 10.72.

Synthesis of $[Mn^{II}(S^{Me2}N_4$(6-Me-DPPN))$](BPh_4)$·MeCN (3). Sodium methoxide (0.11 g, 2.0 mmol), 3-mercapto-3-methyl-2-butanone (0.24 g, 2.0 mmol), and L_3 (0.58 g, 2.0 mmol) were individually dissolved in MeOH (4 mL) and cooled for 30 min at −30 °C in a drybox. The sodium methoxide and 3-mercapto-3-methyl-2-butanone solutions were then combined, and the resulting mixture was allowed to stir at room temperature for another 30 min. This solution was then added dropwise to a Schlenk flask charged with manganese sulfate monohydrate (0.35 g, 2.0 mmol) and a stirbar. The methanolic solution of L_3 was then added dropwise, producing a dark yellow mixture that was allowed to stir at room temperature overnight. Sodium tetraphenylborate (0.70 g, 2.0 mmol) was dissolved in MeOH (2 mL) and added to the solution, which was then permitted to continue stirring at room temperature for 2 days. At the end of this period, all volatiles were removed in vacuo to afford a dark yellow solid. The solid was triturated with Et_2O (20 mL) via stirring at room temperature for 30 min, followed by recovery of the solid material by filtration. The solid material was then redissolved in MeCN (10 mL) and stirred at room temperature for 1 h. The solution was filtered, and the resulting MeCN solution was concentrated to a minimal volume (3−5 mL). Et_2O (7−8 mL) was carefully layered on top of the MeCN solution, and the two layers were allowed to diffuse together overnight at −30 °C. Filtration of the mixture resulted in **3** as a yellow crystalline solid in 64% yield (0.99 g, 1.3 mmol). Electronic absorption spectrum: λ_{max} (nm) (ε (M^{-1} cm^{-1})): (MeCN): 282(1655); (MeOH): 279(770). IR(Nujol): $\nu_{C=N}$ 1651 cm^{-1}. EPR spectrum (MeOH/EtOH glass): g = 1.99. Redox potential (MeCN, 298 K): $E_{1/2}$ = 520 mV; E_{pa} = 580 mV, E_{pc} = 460 mV vs SCE. Magnetic moment (solid state, 5−300 K): 5.57 μ_B; (solution, MeOH, 298 K): 5.78 μ_B. ESI-MS: Expected m/z for $[C_{22}H_{31}N_4SMn]^+$ = 438.5, found m/z = 438.2. Elemental Analysis for $C_{48}H_{54}BN_5SMn$; Calculated: C, 72.17; H, 6.81; N, 8.77. Found: C, 72.25; H, 6.41; N, 8.67.

Synthesis of $[Mn^{II}(S^{Me2}N_4$(2-QuinoPN))$](PF_6)$·MeCN·Et_2O (4). A procedure similar to that employed in the preparation of **3** was conducted with the following reagent amounts; sodium methoxide (0.11 g, 2.0 mmol), 3-mercapto-3-methyl-2-butanone (0.24 g, 2.0 mmol), L_4 (0.73 g, 2.0 mmol), manganese sulfate monohydrate (0.34 g, 2.0 mmol), and sodium hexafluorophosphate (0.34 g, 2.0 mmol). Complex **4** was isolated as a dark orange crystalline solid in 71% yield (0.95 g, 1.5 mmol). Electronic absorption spectrum: λ_{max} (nm) (ε (M^{-1} cm^{-1})) (MeCN): 320(2570); (MeOH): 321(1070). IR (Nujol): $\nu_{C=N}$ 1603 cm^{-1}. EPR spectrum (MeOH,EtOH glass): g = 1.98. Redox potential (MeCN vs SCE): E_{pa}= 525 mV. Magnetic moment (solid state, 5−300 K): 5.91 μ_B; (solution, MeOH, 298 K): 5.98 μ_B. ESI-MS: Expected m/z for $[C_{28}H_{31}N_4SMn]^+$ = 510.6, found m/z = 510.3. Elemental Analysis for $C_{28}H_{31}N_4F_6PSMn$; Calculated: C, 51.30; H, 4.77; N, 8.55. Found: C, 51.46; H, 5.00; N, 8.64.

Synthesis of $[Mn^{II}(S^{Me2}N_4$(6-H-DPEN)(MeOH))$](BPh_4)$ (5). A procedure similar to that employed in the preparation of **1** was conducted with the following reagent amounts: sodium methoxide (0.10 g, 1.9 mmol), 3-mercapto-3-methyl-2-butanone (0.22 g, 1.9 mmol), L_5 (0.43 g, 1.8 mmol), manganese sulfate monohydrate (0.30 g, 1.8 mmol), and sodium tetraphenylborate (0.61 g, 1.8 mmol). **5** was isolated as a white solid in 21% yield (0.28 g, 0.37 mmol). Electronic absorption spectrum (MeCN): λ_{max} (nm) (ε (M^{-1} cm^{-1})): 283(1690). IR (Nujol): $\nu_{C=N}$ 1600 cm^{-1}. EPR spectrum (MeOH,EtOH glass): g = 1.99. Redox potential (MeCN vs SCE, 298 K): E_{pa} = 413 mV, E_{pc} = 0 mV. Magnetic moment (solid state, 5−300 K): 5.88 μ_B; (solution, MeOH, 298 K): 5.79 μ_B. ESI-MS: Expected m/z for $[C_{19}H_{25}N_4SMn]^+$ = 395.9, found m/z = 396.5.

Synthesis of $[Mn^{III}(S^{Me2}N_4$(6-Me-DPEN)$]_2$-(μ-O)$(BF_4)_2$·2MeOH (6). **1** (0.500 g, 0.48 mmol) was dissolved in MeCN (5 mL) and allowed to stir in air for 30 min, during which time the solution turned from yellow to dark purple. The purple solution was then added dropwise into pentane (10 mL), causing the immediate precipitation of a purple solid. The solid material was isolated via filtration, redissolved in MeCN (2 mL), and carefully layered with Et_2O (10 mL). The mixture was allowed to diffuse together at room temperature overnight, resulting in dark purple crystals suitable for X-ray diffraction studies in 97% yield (0.49 g, 0.47 mmol). Electronic absorption spectrum (MeCN): λ_{max} (nm) (ε (M^{-1} cm^{-1})): 325(3690), 557(520). IR (Nujol): $\nu_{C=N}$ 1602 cm^{-1}. Redox potential (MeCN vs SCE, 298 K): $E_{1/2}$= +465 mV. ESI-MS: Expected m/z for $[C_{42}H_{58}N_8OS_2Mn_2]^{2+}$ = 432.5, found m/z = 432.6. Elemental Analysis for $C_{44}H_{66}B_2N_8O_3F_8S_2Mn_2$; Calculated: C, 47.93; H, 6.03; N, 10.16. Found: C, 46.18; H, 5.62; N, 10.34.

Synthesis of $[Mn^{III}(S^{Me2}N_4$(2-QuinoEN)$]_2$-(μ-O)$(PF_6)_2$·Et_2O (7). A procedure similar to that employed in the preparation of **7** was conducted with the following reagent amounts; **2** (0.50 g, 0.78 mmol). **7** was obtained as a dark purple solid in 98% yield (0.50 g, 0.38 mmol). Electronic absorption spectrum: λ_{max} (nm) (ε (M^{-1} cm^{-1})) (MeCN): 345(3450), 562(550); (MeOH): 332(2000), 606(240). IR (Nujol):

dx.doi.org/10.1021/ic300192q | Inorg. Chem. 2012, 51, 6633−6644

$\nu_{C=N}$ 1603 cm^{-1}. Redox potential (MeCN vs SCE, 298 K): E_{pa}= +780 mV (irrev). ESI-MS: Expected m/z for $[C_{54}H_{58}N_8OS_2Mn_2]^{2+}$ = 504.5, found m/z = 504.4. Elemental Analysis for $C_{54}H_{58}N_8OF_{12}P_2S_2Mn_2$ Calculated: C, 49.93; H, 4.50; N, 8.63. Found: C, 50.93; H, 4.63; N, 8.77.

Synthesis of $[Mn^{III}(S^{Me2}N_4$(6-Me-DPPN))$]_2(\mu$-O)$(BPh_4)_2$ (8). An 8 mL EtCN solution of **3** (0.200 g, 0.26 mmol) was prepared under an inert atmosphere in a drybox. The resulting yellow solution was removed from the drybox, cooled to −80 °C, and exposed to air overnight. During this period the solution was found to turn from yellow to dark brown. Cold Et_2O (−80 °C, 10 mL) was carefully layered on top of the EtCN solution, and the resulting mixture was maintained at −80 °C for a few weeks to permit the formation of small crystals suitable for X-ray diffraction studies. Electronic absorption spectrum (MeCN): λ_{max} (nm) (ε (M^{-1} cm^{-1})): 374 (750), 594 (190). ESI-MS: Expected m/z for $[C_{44}H_{62}N_8OS_2Mn_2]^{2+}$ = 446.5, found m/z = 446.3.

Synthesis of $[Mn^{III}(S^{Me2}N_4$(2-QuinoPN))$]_2(\mu$-O)$(BPh_4)_2$ (9). A procedure similar to that described for the synthesis of **8** was employed with a 4 mL EtCN solution of the BPh_4^- salt of **4** (0.400 g, 0.482 mmol). Small gray crystals of **9** were obtained in extremely low yields from crystallization attempts. Electronic absorption spectrum (MeCN): λ_{max} (nm): 388, 573 (br). ESI-MS: Expected m/z for $[C_{56}H_{62}N_8OS_2Mn_2]^{2+}$ = 518.6, found m/z = 518.3.

Synthesis of $[Mn^{III}(S^{Me2}N_4$(6-H-DPEN)$]_2(\mu$-O)$(PF_6)_2\cdot(MeCN)_2$ (10). A procedure similar to that employed in the preparation of **6** was conducted with $[Mn^{II}(S^{Me2}N_4$(6-H-DPEN)(MeOH)$](PF_6)$ (0.20 g, 0.35 mmol). **10** was obtained as a light purple solid in 95% yield (0.19 g, 0.17 mmol). Electronic absorption spectrum: λ_{max} (nm) (ε (M^{-1} cm^{-1})) (MeCN): 327 (4463), 332 (4470), 533 (286). IR (Nujol): $\nu_{C=N}$ 1600 cm^{-1}. Magnetic moment (solid state, 300 K): 4.89 μ_B/Mn; (solution, MeOH, 298 K): 4.01 μ_B/Mn. Redox potential (MeCN vs SCE, 298 K): $E_{1/2}$= +295 mV. ESI-MS: Expected m/z for $[C_{38}H_{50}N_8OS_2Mn_2]^{2+}$ = 404.3, found m/z = 404.3. Elemental Analysis for $C_{38}H_{50}N_8OF_{12}P_2S_2Mn_2$ Calculated: C, 41.54; H, 4.59; N, 10.20. Found: C, 41.31; H, 4.68; N, 10.36.

Alternative Synthetic Route to 6, 7, and 10 Using Iodosylbenzene. Addition of 1.1 equiv of solid iodosylbenzene to a saturated MeCN solution (2−4 mL typical volume) of either **1**, **2**, or **5** under an inert atmosphere resulted in the immediate formation of **6**, **7**, or **10**, respectively. The remaining solids were removed by filtration, and the resulting MeCN solution was added dropwise into pentane (10 mL) to precipitate the desired product. Isolation of the precipitated solid material via filtration resulted in yields very close to those using O_2.

X-ray Crystallographic Structure Determination. A red prism of **1** with dimensions 0.48 × 0.29 × 0.24 mm^3 was mounted on a glass capillary with oil. Data was collected at −143 °C. The crystal-to-detector distance was set to 40 mm, and the exposure time was 60 s per degree for three total sets of exposure. The scan width was set to 1.0°. Data collection was 90.7% complete to 29.53° in ϑ and 99.6% complete to 25°. A total of 32,825 partial and complete reflections were collected covering the indices h = −13 to 13, k = −19 to 19, l = −22 to 22. 5,980 reflections were symmetry independent and the R_{int} = 0.038 indicated that the data was above average quality (0.07). Indexing and unit cell refinement indicated an orthorhombic lattice with the space group $P2_12_12_1$ (No. 19).

A pale-yellow prism of **3** with dimensions 0.20 × 0.17 × 0.10 mm^3 was mounted on a glass capillary with oil. Data was collected at −163 °C. The crystal-to-detector distance was set to 40 mm, and the exposure time was 20 s per degree for all sets of exposure. The scan width was 0.5°. Data collection was 98.7% complete to 25.0° in ϑ. A total of 114,668 merged reflections were collected covering the indices h = −17 to 17, k = −20 to 20, l = −22 to 22. A total of 16,232 reflections were symmetry independent, and the R_{int} = 0.0343 indicated that the data was good (0.07). Indexing and unit cell refinement indicated a triclinic P lattice with the space group $P\bar{1}$ (No. 2).

A brown prism of **4** with dimensions 0.18 × 0.15 × 0.10 mm^3 was mounted on a glass capillary with oil. Data was collected at −163 °C. The crystal-to-detector distance was set to 40 mm, and the exposure time was 20 s per degree for all sets of exposure. The scan width was 0.5°. Data collection was 99.7% complete to 25.0° in ϑ. A total of 61,040 merged reflections were collected covering the indices h = −18 to 17, k = −23 to 20, l = −21 to 22. A total of 8,766 reflections were symmetry independent, and the R_{int} = 0.0432 indicated that the data was good (0.07). Indexing and unit cell refinement indicated a primitive monoclinic lattice with the space group $P2_1/n$ (No. 14). The complex and counterion are accompanied by a 2:1 mixture of MeCN and Et_2O that occupy the same space. The associated disorder required a few stabilizing restraints to ensure convergence of the thermal parameters for the three solvents molecules.

A yellow crystal of **5** was cut down to dimensions 0.6 × 0.6 × 0.6 mm^3 and mounted on a glass capillary with oil. Data was collected at −143 °C. The crystal-to-detector distance was set to 30 mm, and the exposure time was 15 s per degree for all sets of exposure. The scan width was 2.0°. Data collection was 98.5% complete to 25.0° in ϑ. A total of 48881 merged reflections were collected covering the indices h = −13 to 13, k = −19 to 19, l = −19 to 19. A total of 7339 reflections were symmetry independent, and the R_{int} = 0.039 indicated that the data was better than average quality (0.07). Indexing and unit cell refinement indicated a triclinic P-lattice with the space group $P\bar{1}$ (No. 2).

A black block of **6** with dimensions 0.30 × 0.20 × 0.15 mm^3 was mounted on a glass capillary with oil. Data was collected at −173 °C. The crystal-to-detector distance was set to 40 mm, and the exposure time was 10 s per degree for all sets of exposure. The scan width was 0.5°. Data collection was 98.7% complete to 25.0° in ϑ. A total of 21,006 merged reflections were collected covering the indices h = −16 to 13, k = −23 to 24, l = −9 to 14. A total of 5,905 reflections were symmetry independent, and the R_{int} = 0.041 indicated that the data was excellent (0.07). Indexing and unit cell refinement indicated a monoclinic P lattice with the space group $P2_1/c$ (No. 14). One methanol molecule was found with half-site occupancy in the structure.

A crystal of **7** with dimensions 0.30 × 0.07 × 0.05 mm^3 was mounted on a glass capillary with oil. Data was collected at −173 °C. The crystal-to-detector distance was set to 49.4 mm, and the exposure time was 20 s per degree for all sets of exposure. Data collection was 99.0% complete to 27.50° in ϑ. A total of 29,448 reflections were collected covering the indices h = −26 to 26, k = −29 to 28, l = −17 to 16. A total of 6,872 reflections were symmetry independent with R_{int} = 0.0553. Indexing and unit cell refinement indicated a monoclinic lattice with the space group $C2/c$.

A colorless plate of **8** with dimensions 0.30 × 0.20 × 0.15 mm^3 was mounted on a glass capillary with oil. Data was collected at −173 °C. The crystal-to-detector distance was set to 40 mm, and the exposure time was 10 s per degree for all sets of exposure. The scan width was 0.5°. Data collection was 99.7% complete to 28.36° in ϑ. A total of 123,964 merged reflections were collected covering the indices h = −38 to 38, k = −15 to 15, l = −33 to 34. A total of 10,165 reflections were symmetry independent, and the R_{int} = 0.0732 indicated that the data was acceptable (average quality 0.07). Indexing and unit cell refinement indicated a monoclinic C lattice with the space group $C2/c$ (No. 15).

A crystal of **9** cut to dimensions 0.10 × 0.10 × 0.05 mm^3 was mounted on a glass capillary with oil. Data was collected at −173 °C. The crystal-to-detector distance was set to 40 mm, and the exposure time was 60 s per degree for all sets of exposure. The scan width was 1.0°. Data collection was 49.5% complete to 20° in ϑ. A total of 69,414 reflections were collected covering the indices h = −25 to 25, k = −49 to 48, l = −14 to 14. A total of 9,478 reflections were symmetry independent with R_{int} = 0.6592. Indexing and unit cell refinement indicated a monoclinic P lattice with the space group $P2_1/c$ (No.14).

A plate of **10** was cut to dimensions 0.59 × 0.40 × 0.40 mm^3 was mounted on a glass capillary with oil. Data was collected at −173 °C. The crystal-to-detector distance was set to 30 mm, and the exposure time was 45 s per degree for all sets of exposure. The scan width was 1.0°. Data collection was 99.3% complete to 25° in ϑ. A total of 78,553 reflections were collected covering the indices h = −21 to 21, k = −26

dx.doi.org/10.1021/ic300192q | Inorg. Chem. 2012, 51, 6633−6644

Table 1. Crystal Data for $[Mn^{II}(S^{Me2}N_4(6\text{-Me-DPEN})](PF_6)$ (1), $[Mn^{II}(S^{Me2}N_4(6\text{-Me-DPPN})](BPh_4)\cdot MeCN$ (3), $[Mn^{II}(S^{Me2}N_4(2\text{-QuinoPN}))](PF_6)\cdot MeCN\cdot Et_2O$ (4), $[Mn^{II}(S^{Me2}N_4(6\text{-H-DPEN})(MeOH)](BPh_4)\cdot MeOH$ (5), $[Mn^{III}(S^{Me2}N_4(6\text{-Me-DPEN})]_2(\mu\text{-O})(BF_4)_2\cdot 2MeOH$ (6), $[Mn^{III}(S^{Me2}N_4(2\text{-QuinoEN})]_2(\mu\text{-O})(PF_6)_2\cdot Et_2O$ (7), and $[Mn^{III}(S^{Me2}N_4(6\text{-Me-DPPN}))]_2(\mu\text{-O})(BPh_4)_2$ (8), $[Mn^{III}(S^{Me2}N_4(2\text{-QuinoPN}))]_2(\mu\text{-O})(BPh_4)_2\cdot MeCN$ (9), and $[Mn^{III}(S^{Me2}N_4(6\text{-H-DPEN})]_2(\mu\text{-O})(PF_6)_2\cdot 2MeCN$ (10)

	1	3	4	5	6	7	8	9	10
formula	$C_{21}H_{29}F_6MnN_4PS_1$	$C_{48}H_{54}BMnN_5S$	$C_{64}H_{78}F_{12}Mn_2N_{10}OP_2S_2$	$C_{46}H_{57}BMnN_4O_3S$	$C_{43}H_{62}B_2F_8Mn_2N_8O_2S_2$	$C_{58}H_{68}F_{12}Mn_2N_8OP_4S$	$C_{92}H_{102}B_2Mn_2N_8OS_2$	$C_{106}H_{105}B_2Mn_2N_9OS_2$	$C_{158}H_{209}F_{48}Mn_8N_{35}O_4P_8S_8$
MW	569.46	798.77	1467.30	811.77	1070.63	1387.02	1531.46	1716.61	4518.36
T, K	130(2)	110(2)	110(2)	130(2)	90.0(5)	100(2)	100(2)	100(2)	130(2)
unit cell[a]	orthorhrombic	triclinic	monoclinic	triclinic	monoclinic	monoclinic	monoclinic	monoclinic	orthorhombic
a, Å	10.2775 (2)	11.4076 (2)	13.8606 (2)	9.8409(2)	12.1000 (8)	20.3410 (5)	28.987(2)	25.110(7)	17.7825(3)
b, Å	14.7368 (3)	13.3193 (2)	15.4379 (2)	14.7102(3)	18.4235 (13)	23.0106 (6)	11.4787(7)	48.999(14)	22.2270(4)
c, Å	16.0656 (3)	14.7867 (2)	16.6849 (3)	14.9428(3)	10.9203 (8)	13.7451 (4)	25.501(2)	14.589(6)	12.5151(7)
α, deg	90	90.4060 (10)	90	96.6399(7)	90	90	90	90	90
β, deg	90	105.2960(10)	108.2020 (10)	94.6004(7)	96.947 (2)	110.4220(10)	105.896(7)	89.56(8)	90
γ, deg	90	101.1620 (10)	90	97.0075(10)	90	90	82.8680(10)	14.589(6)	90
V, Å^3	2433.25(8)	2122.11 (6)	3391.56 (9)	2122.80(7)	2416.5 (3)	6030.7 (3)	8160.5(10)	17949(10)	4946.6(3)
Z	4	2	2	2	2	4	4	4	1
d(calc), g/cm^3	1.554	1.250	1.436	1.270	1.471	1.528	1.238	0.635	1.517
space group	P $2_12_12_1$	P $\bar{1}$	P $2_1/n$	P $\bar{1}$	P $2_1/c$	C 2/c	C 2/c	P $2_1/c$	P 2_12_12
R	0.0364[b]	0.0413[b]	0.0390[b]	0.0505[b]	0.0538[b]	0.0525[b]	0.0413[b]	0.1630[b]	0.0559[b]
R_w	0.0941[c]	0.1091[c]	0.0933[c]	0.1499[c]	0.1499[c]	0.1562[c]	0.1019[c]	0.4681[c]	0.1381[c]
GOF	1.018	1.020	1.013	1.071	1.020	1.049	0.964	1.044	0.969

[a]In all cases: Mo Kα(λ = 0.71070 Å) radiation. [b]$R = \sum||F_o| - |F_c||/\sum|F_o|$; $R_w = [\sum w(|F_o| - |F_c|)^2/\sum wF_o^2]^{1/2}$, where $w^{-1} = [\sigma_{count}^2 + (0.05F^2)^2]/4F^2$.

dx.doi.org/10.1021/ic300192q | Inorg. Chem. 2012, 51, 6633−6644

Table 2. Selected Bond Distances (Å) and Bond Angles (deg) for $[Mn^{II}(S^{Me2}N_4(6\text{-Me-DPEN})](PF_6)$ (1), $[Mn^{II}(S^{Me2}N_4(2\text{-QuinoEN}))](PF_6)$ (2), $[Mn^{II}(S^{Me2}N_4(6\text{-Me-DPPN})](BPh_4)$ (3), $[Mn^{II}(S^{Me2}N_4(2\text{-QuinoPN}))](PF_6)$ (4), $[Mn^{II}(S^{Me2}N_4(6\text{-H-DPEN})(MeOH)](BPh_4)\cdot MeOH$ (5), $[Mn^{III}(S^{Me2}N_4(6\text{-Me-DPEN})]_2(\mu\text{-O})(BF_4)_2$ (6), $[Mn^{III}(S^{Me2}N_4(2\text{-QuinoEN})]_2(\mu\text{-O})(PF_6)_2$ (7), $[Mn^{III}(S^{Me2}N_4(6\text{-Me-DPPN}))]_2(\mu\text{-O})(BPh_4)_2$ (8), and $[Mn^{III}(S^{Me2}N_4(6\text{-H-DPEN})]_2(\mu\text{-O})(PF_6)_2\cdot 2MeCN$ (10)

	1	2	3	4	5	6	7	8	10
Mn−S(1)	2.3710(6)	2.3835(9)	2.3742(3)	2.3626 (5)	2.4597(6)	2.2767(7)	2.292(1)	2.2547(16)	2.2968(15)
Mn−N(1)	2.186(2)	2.170(2)	2.1909(10)	2.2106 (15)	2.2215(16)	1.999(3)	2.010(3)	2.0660(16)	2.011(4)
Mn−N(2)	2.297(2)	2.274(2)	2.2476(10)	2.2424 (16)	2.3595(16)	2.151(2)	2.130(3)	2.2008(16)	2.190(4)
Mn−N(3)	2.222(2)	2.225(3)	2.1830(10)	2.1886 (16)	2.2790(18)	2.581(2)	2.543(3)	2.3524(16)	2.243(5)
Mn−N(4)	2.239(2)	2.200(3)	2.2787(10)	2.2689 (14)	2.2463(17)	2.501(2)	2.370(3)	2.796	2.223(5)
Mn(1)−O(1)	N/A	N/A	N/A	N/A	2.183(1)[a]	1.7602(4)	1.7599(6)	1.7941(6)	1.771(4)
Mn(1′)−O(1)	N/A	N/A	N/A	N/A	N/A	1.7602(4)	1.7599 (6)	1.7941(6)	1.750(4)
Mn(1)···Mn(1′)	N/A	N/A	N/A	N/A	N/A	3.520	3.512	3.433	3.515
S(1)−Mn−N(1)	81.15(5)	82.20(7)	82.03(3)	82.66(4)	78.77(4)	82.08(8)	82.60 (8)	82.43(5)	83.4(1)
S(1)−Mn−N(2)	156.98(5)	156.10(7)	154.06(3)	155.06(4)	155.39(4)	164.17(7)	163.90(9)	169.44(5)	164.2(1)
S(1)−Mn−N(3)	117.36(5)	106.98(7)	127.47(3)	124.91(5)	108.79(5)	106.19(6)	101.40(8)	117.64(5)	101.2(1)
S(1)−Mn−N(4)	117.38(5)	123.09(7)	93.97(3)	100.31(4)	108.23(4)	106.84(6)	109.23(8)	N/A	106.6(1)
N(1)−Mn−N(3)	121.37(7)	118.53(9)	114.15(4)	104.28(6)	84.76(6)	86.85(6)	94.92(11)	86.81(6)	86.81(6)
N(1)−Mn−N(4)	120.58(7)	119.04(9)	140.58(4)	152.29(6)	104.19(6)	92.68(13)	84.75(11)	N/A	84.4(1)
N(3)−Mn−N(4)	100.00(7)	104.16(9)	99.40(4)	96.55(5)	142.93(6)	146.57(6)	149.03(10)	N/A	151.7(2)
S(1)−Mn−O(1)	N/A	N/A	N/A	N/A	97.35(4)[a]	95.37(2)	99.20(3)	89.99(4)	98.9(1)
N(1)−Mn−O(1)	N/A	N/A	N/A	N/A	171.07(6)[a]	177.21(9)	177.02(12)	172.35(6)	176.5(2)
Mn−O(1)−Mn	N/A	N/A	N/A	N/A	N/A	180.0	172.3(2)	146.15(11)	173.0(2)
τ-value	0.59	0.55	0.22	0.05	0.47	N/A	N/A	N/A	N/A

[a]In this case, O(1) = MeOH oxygen.

to 26, l = −15 to 19. A total of 910 reflections were symmetry independent with R_{int} = 0.114. Indexing and unit cell refinement indicated a orthorhombic P lattice with the space group $P2_12_12$ (No.18).

A red plate of **11** cut to dimensions 0.50 × 0.30 × 0.10 mm^3 was mounted on a glass capillary with oil. Data was collected at −143 °C. The crystal-to-detector distance was set to 30 mm, and the exposure time was 20 s per degree for all sets of exposure. The scan width was 2.0°. Data collection was 98.0% complete to 25° in ϑ. A total of 68,741 reflections were collected covering the indices h = −21 to 21, k = −28 to 27, l = −19 to 18. A total of 10,722 reflections were symmetry independent with R_{int} = 0.1380. Indexing and unit cell refinement indicated a monoclinic C lattice with the space group Cc (No.9).

The data for **1**, **5**, **10**, and **11** were integrated and scaled using hkl-SCALEPACK. Data for **3**, **4**, **6**, **7**, **8**, and **9** were integrated and scaled using SAINT, SADABS within the APEX2 software package by Bruker, and solutions were made by direct methods (SHELXS, SIR97) to produce complete heavy atom phasing models. Structures were completed by difference Fourier synthesis with SHELXL97 or SHELXTL 6.10 (7). All non-hydrogen atoms were refined anistropically by full-matrix least-squares methods, while all hydrogen atoms were placed using a riding model. Crystal data for **1** and **3**−**10** are summarized in Table 1 below and metrical parameters for **1**−**8** and **10** are provided in Table 2. A complete list of the crystal data and metrical parameters for **11** are provided in the Supporting Information.

RESULTS AND DISCUSSION

Syntheses and Structural Characterization of Complexes 1−5. Ligand scaffolds containing various combinations of N-heterocyclic moieties (pyridine, 6-methyl-pyridine, quinoline) and alkyl spacers (ethyl, propyl) used in this study were constructed via the synthetic route shown in Scheme 1. Maintaining a single primary amine in L_1−L_5 was a key prerequisite to forming the desired thiolate-containing ligands, which are constructed via Mn(II)-templated Schiff-base condensations between the primary amine and 3-mercapto-3-methyl-2-butanone. The alkyl thiolate ligated complexes $[Mn^{II}(S^{Me2}N_4(6\text{-Me-DPEN})](PF_6)$ (**1**), $[Mn^{II}(S^{Me2}N_4(2$-

Scheme 1[a]

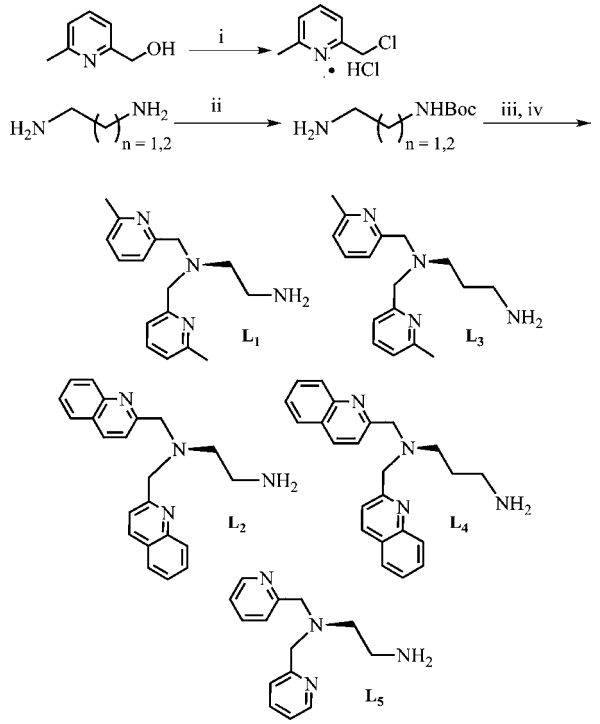

[a]Reaction conditions: (i) 6.0 equiv of $SOCl_2$, CH_2Cl_2, inert atmosphere (N_2), 0 °C → ambient temperature, 16 h. (ii) 0.17 equiv of Boc_2O, CH_2Cl_2, inert atmosphere (N_2), ambient temperature, 24 h; (iii) 1.7−1.9 equiv of 2-(chloromethyl)-6-methylpyridine hydrochloride (L_1 and L_3), 2-(chloromethyl)quinoline hydrochloride (L_2 and L_4), or 2-(chloromethyl)-pyridine hydrochloride (L_5), 5 M NaOH (aq), room temperature, 3−5 days; (iv) 10−32 equiv of trifluoroacetic acid, CH_2Cl_2, 12 h.

dx.doi.org/10.1021/ic300192q | Inorg. Chem. 2012, 51, 6633−6644

QuinoEN))](PF$_6$) (**2**), [Mn^{II}(S^{Me2}N$_4$(6-Me-DPPN)](BPh$_4$)·MeCN (**3**), [Mn^{II}(S^{Me2}N$_4$(2-QuinoPN))](PF$_6$)·MeCN·Et$_2$O (**4**), and [Mn^{II}(S^{Me2}N$_4$(6-H-DPEN)(MeOH)](BPh$_4$)·MeOH (**5**) were all prepared in a similar fashion by combining equimolar amounts of $MnSO_4·H_2O$, ligands L_1–L_5 (respectively), NaOMe, 3-methyl-3-mercapto-2-butanone, and either $NaBF_4$, $NaPF_6$, or $NaBPh_4$ in MeOH, under an inert atmosphere. This general method is analogous to that employed previously by our group for the synthesis of a variety of divalent thiolate-ligated transition metal complexes built upon the *tris*(2-aminoethyl)amine (tren) ligand scaffold.[38,39] Selected metrical parameters for complexes **1**–**5** are assembled in Table 2. The X-ray structure of **2** was reported elsewhere.[13]

As shown in the ORTEP diagrams of Figure 1, monocationic complexes **1**, **3**, and **4** are five-coordinate complexes despite

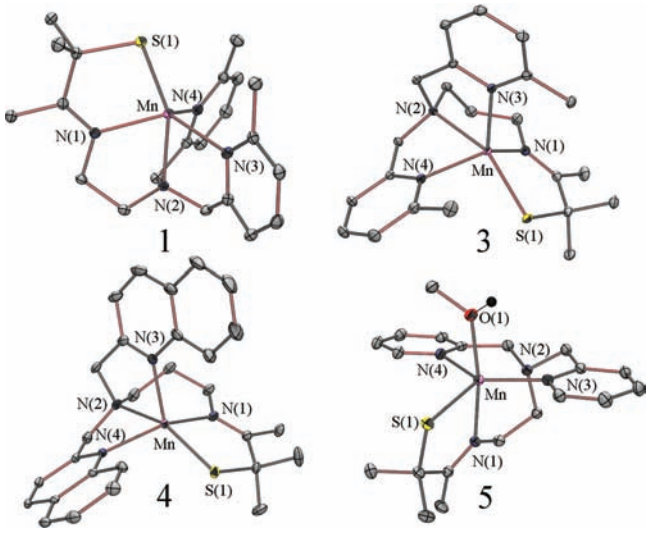

Figure 1. ORTEP diagrams of [Mn^{II}(S^{Me2}N$_4$(6-Me-DPEN))]$^+$ (**1**), [Mn^{II}(S^{Me2}N$_4$(6-Me-DPPN))]$^+$ (**3**), [Mn^{II}(S^{Me2}N$_4$(2-QuinoPN))]$^+$ (**4**), and [Mn^{II}(S^{Me2}N$_4$(6-H-DPEN)(MeOH)]$^+$ (**5**) with counterions, solvents of crystallization, and hydrogen atoms omitted.

being synthesized and crystallized from coordinating solvents (MeOH or MeCN). These observations are consistent with the X-ray crystal structure of previously reported five-coordinate **2**.[13] The primary coordination spheres of each complex contain a thiolate sulfur (S(1)), imine nitrogen (N(1)), tertiary amine (N(2)), and two N-heterocyclic moieties (N(3) and N(4)). Complex **5**, on the other hand, was found to contain a methanol ligand bound in an available coordination site *trans* to the imine nitrogen (Figure 2). The presence of a single counterion per Mn complex in the X-ray crystal structure of **5** supports the assignment of this exogenous ligand as methanol and not methoxide.

Close inspection of the metrical parameters (Table 2) for methanol-bound **5** reveals a fairly dramatic elongation of the Mn·····N(2) separation (2.3595(16) Å) to the point where it is nearly 0.07 Å longer than the sum of the ionic radii for these two atoms (2.29 Å).[44] Complex **5** is, therefore, also *best* described as a five-coordinate complex. This particular compound is further distinguished in that the pyridine moieties in this complex are unsubstituted and therefore impose less steric congestion upon the open coordination site than do the 6-methylpyridine or quinoline moieties of **1**–**4** (Figure 2).

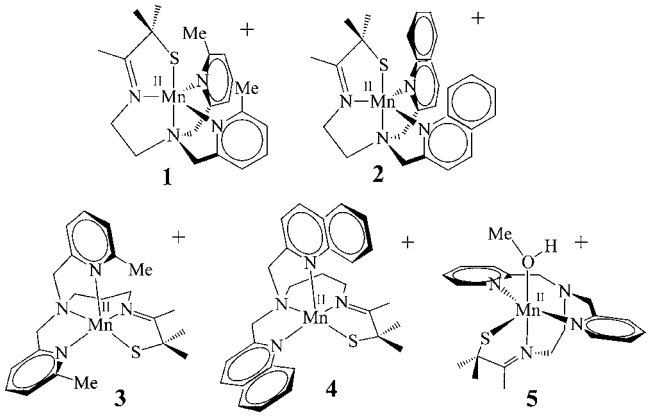

Figure 2. Chemdraw diagrams of [Mn^{II}(S^{Me2}N$_4$(6-Me-DPEN))]$^+$ (**1**), [Mn^{II}(S^{Me2}N$_4$(2-QuinoEN))]$^+$ (**2**), [Mn^{II}(S^{Me2}N$_4$(6-Me-DPPN))]$^+$ (**3**), [Mn^{II}(S^{Me2}N$_4$(2-QuinoPN))]$^+$ (**4**), and [Mn^{II}(S^{Me2}N$_4$(6-H-DPEN)(MeOH)]$^+$ (**5**).

Substitution of the pyridine 6-position has been found in a number of cases to have dramatic effects upon the properties and reactivity of various small molecule compounds containing first-row transition metals.[45–47] Solvent coordination to **5** is presumably more facile due to the absence of these bulkier substituents. The coordination geometries of complexes **1**–**5** are found to vary from distorted trigonal bipyramidal to square pyramidal (τ(**1**) = 0.59, τ(**2**) = 0.55, τ(**3**) = 0.22, τ(**4**) = 0.05, and τ(**5**) = 0.47),[48] indicating that modification of the alkyl spacer length from an ethylene (**1**, **2**, and **5**) to propylene (**3** and **4**) unit (Figure 2) has a considerable impact upon the coordination geometry. This effect has previously been observed when comparing the structures of five-coordinate *bis*-thiolate-ligated [Fe^{III}(S$_2$^{Me2}N$_3$(Et,Pr))]$^+$ and [Fe^{III}(S$_2$^{Me2}N$_3$(Pr,Pr))]$^+$, although the addition of an extra methylene unit in the latter complex was found to promote a more trigonal bipyramidal geometry.[49]

The Mn–S(1) bond distances in complexes **1**–**4** range from 2.3710(6) Å to 2.3835(9) Å (Table 2), and are very similar to the Mn–SR bonds found in aromatic thiolate-ligated [Mn^{II}$_4$(SPh)$_{10}$]^{50} and [Mn^{II}{HB-(3,5-Me$_2$pz)$_3$}(SC$_6$F$_5$)]^{51} (Mn–SR = 2.38(1) Å (mean length) and 2.385(3) Å, respectively), but shorter than those found in alkyl thiolate-ligated [Mn^{II}(edt)$_2$]$^{2-}$ and [Mn^{II}(S^{Me2}N$_4$(tren))]$^+$ (Mn–SR = 2.432(7)Å and 2.412(3) Å, respectively).[39,50] The π-accepting N-heterocyclic moieties found in **1**–**4** should increase the metal ion Lewis acidity relative to the structurally analogous aliphatic primary amine-ligated [Mn^{II}(S^{Me2}N$_4$(tren))]$^+$, which explains the contraction of the Mn–S(1) bonds in **1**–**4** versus [Mn^{II}(S^{Me2}N$_4$(tren))]$^+$. Complex **5** has a longer Mn–S(1) (2.4597(6) Å) bond relative to **1**–**4** due presumably to the coordination of methanol (Table 2). The spin-states of complexes **1**–**5** are all identical.

Magnetic, Spectroscopic, and Electrochemical Properties of Complexes 1–5. Fits to variable temperature solid-state magnetic susceptibility data show that complexes **1**–**5** each contain high-spin Mn(II) ions, as illustrated for complex **1** in Figure 3a. Each complex exhibits Curie behavior from 5 to 300 K (Figures 3a, Supporting Information, Figures S-20, S-25)[13] with calculated effective magnetic moments between 5.57 μB and 5.91 μB, which is close to the theoretical spin-only value (5.92 μB) for a S = 5/2 system. Solution magnetic moments obtained using the Evans method in MeOH solution

dx.doi.org/10.1021/ic300192q | *Inorg. Chem.* 2012, 51, 6633–6644

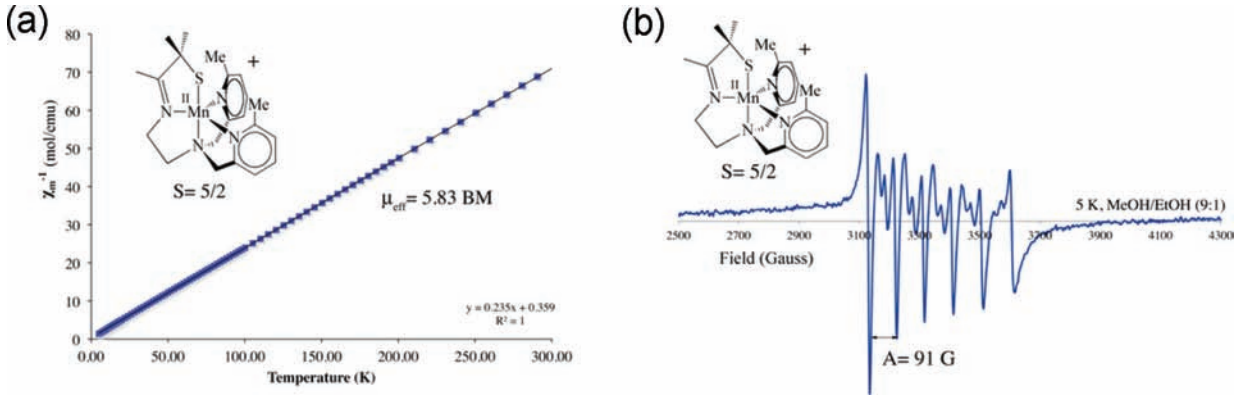

Figure 3. Inverse molar magnetic susceptibility (χ_M^{-1}) vs temperature (T) plot (a) for $[Mn^{II}(S^{Me2}N_4(6\text{-MeDPEN}))](BF_4)$ (**1**) showing Curie behavior consistent with an $S = 5/2$ ground spin-state. X-band EPR spectrum (b) of $[Mn^{II}(S^{Me2}N_4(6\text{-MeDPEN}))](BF_4)$ (**1**) in MeOH/EtOH (9:1) glass at 7 K.

were very similar to the solid-state data (see Experimental Section). As illustrated in Figure 3b for complex **1**, low temperature (4−7 K) X-band EPR spectra of **1**−**5** (Supporting Information, Figures S-24, and S-29)[13] display similar six-line signals with g-values of approximately 2.00 and hyperfine splitting constants ranging from 90 to 100 G, again consistent with monomeric high-spin ($S = 5/2$) Mn(II) ($I_{Mn} = 5/2$). The electronic absorption spectrum of each complex (Supporting Information, Figures S-16, S-18, S-22, S-27) was found to be featureless throughout the visible region in a wide range of solvents (MeCN, EtCN, MeOH, CH_2Cl_2). This is expected given that the ligand field transitions are both Laporté and spin forbidden for an $S = 5/2$ spin system. The absence of intense $S(\pi)\rightarrow Mn(d)$ charge transfer bands in the visible region implies that these transitions occur at higher energy (UV region), in agreement with Solomon's spectral analysis of four-coordinate $[Mn^{II}\{HB(3,5\text{-}^{i}Pr_2pz\}_3(SC_6F_5)]$.[52] Ligand-centered $\pi\rightarrow\pi^*$ transitions involving the imine and N-heterocyclic moieties likely contribute to the absorption features observed in the near UV spectral region of each complex (see Experimental Section).

The electrochemical properties of **1**−**5** were examined using cyclic voltammetry in MeCN at ambient temperature. Complexes **1** (Figure 4) and **3** (Supporting Information, Figure S-21) display reversible and quasireversible Mn(III/II) redox couples at $E_{1/2} = 410$ mV and 520 mV, respectively, while complexes **2**,[13] **4**, and **5** are irreversibly oxidized to the +3 oxidation state (Supporting Information, Figures S-26 and S-30). Given that some of these processes are irreversible, it is difficult to draw any conclusions regarding the N-heterocyclic ligand's influence on redox potential. However, it does appear that the trigonal bipyramidal complexes containing the ethyl linker are easier to oxidize than the square pyramidal complexes containing the propyl linker. No other redox processes, such as a wave attributable to a Mn(IV/III) couple, were observed within the MeCN solvent window. The relatively modest potentials associated with the Mn^{II}/Mn^{III} redox couple (460−580 mV vs SCE) suggest that **1**−**5** could be oxidized by a variety of biological oxidants, including O_2.

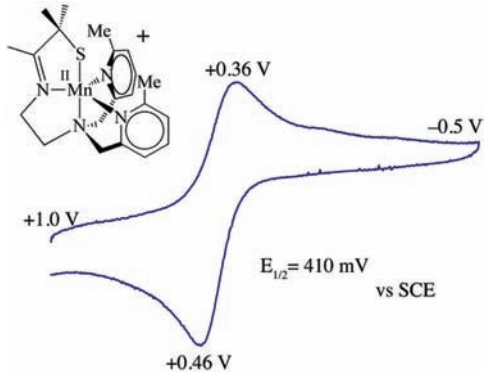

Figure 4. Cyclic voltammogram of $[Mn^{II}(S^{Me2}N_4(6\text{-MeDPEN}))](BF_4)$ (**1**) in MeCN vs SCE with 0.1 M $Bu_4^nPF_6$ supporting electrolyte and scan rate of 150 mV·s^{-1}.

Dioxygen Reactivity of Complexes 1−5. Complexes **1**−**5** were found to be highly reactive with O_2 in organonitrile solvents (MeCN, EtCN), each to afford a rare example of an unsupported oxo-bridged Mn(III) dimer (complexes **6**−**10**). Selected metrical parameters for these complexes, $[Mn^{III}(S^{Me2}N_4(6\text{-Me-DPEN})]_2\text{-}(\mu\text{-O})(BF_4)_2\cdot 2MeOH$ (**6**), $[Mn^{III}(S^{Me2}N_4(QuinoEN)]_2\text{-}(\mu\text{-O})(PF_6)_2\cdot Et_2O$ (**7**), $[Mn^{III}(S^{Me2}N_4(6\text{-Me-DPPN})]_2\text{-}(\mu\text{-O})(BPh_4)_2$ (**8**), $[Mn^{III}(S^{Me2}N_4(QuinoPN)]_2\text{-}(\mu\text{-O})(BPh_4)_2\cdot MeCN$ (**9**), and $[Mn^{III}(S^{Me2}N_4(6\text{-H-DPEN})]_2\text{-}(\mu\text{-O})(PF_6)_2\cdot 2MeCN$ (**10**), are provided either in Table 2 or Supporting Information, Table S-34. Dicationic μ-oxo bridged **6**, **7** (Figure 5), and **10** (Figure 6) were found to be extremely robust; each complex exhibits indefinite stability in both the solid state and solution under ambient conditions. Complexes **8** (Figure 7) and **9** (Supporting Information, Figure S-38), on the other hand, were found to be thermally unstable ($\tau_{1/2}$ for **8** and **9** is ∼15−20 min at −40 °C in MeCN) and rapidly convert to intractable products upon warming to ambient temperature. Because of this, the crystal quality of complex **9** was poor resulting in a less-than desirable resolution ($R = 16\%$) X-ray structure, which does not lend itself to a thorough consideration of metrical parameters. This structure is, however, included in the following discussion primarily to confirm that O_2 addition to **4** results in the formation of an unsupported oxo-bridged dimer.

Only 0.25 equiv of O_2 per equivalent of Mn(II) are required to quantitatively convert **1**, **2**, and **5** to their corresponding μ-oxo dimers **6**, **7**, and **10**, at room temperature on a high-vacuum line (with a calibrated known-volume bulb). Each dimer was isolated in nearly quantitative yields (92−98%), suggesting that metal-centered oxidation is the predominant O_2 reaction pathway, as opposed to sulfur oxidation, which frequently occurs with thiolate-containing transition metal com-

dx.doi.org/10.1021/ic300192q | Inorg. Chem. 2012, 51, 6633−6644

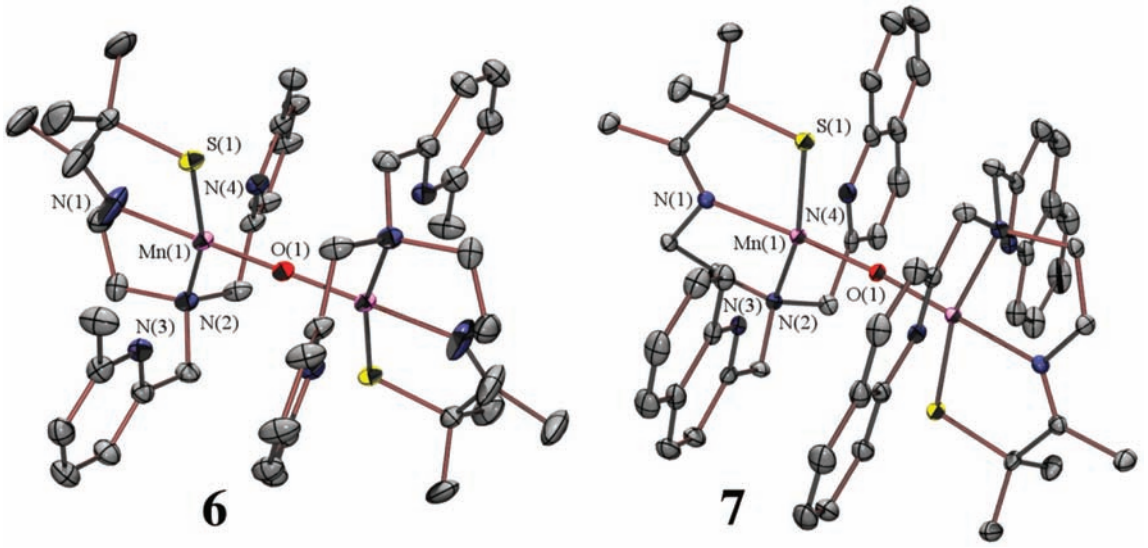

Figure 5. ORTEP diagrams of $\{[Mn^{III}(S^{Me2}N_4(6\text{-Me-DPEN})]_2\text{-}(\mu\text{-O})\}^{2+}$ (**6**) and $\{[Mn^{III}(S^{Me2}N_4(QuinoEN)]_2\text{-}(\mu\text{-O})\}^{2+}$ (**7**) with counterions, solvents of crystallization, and hydrogen atoms omitted.

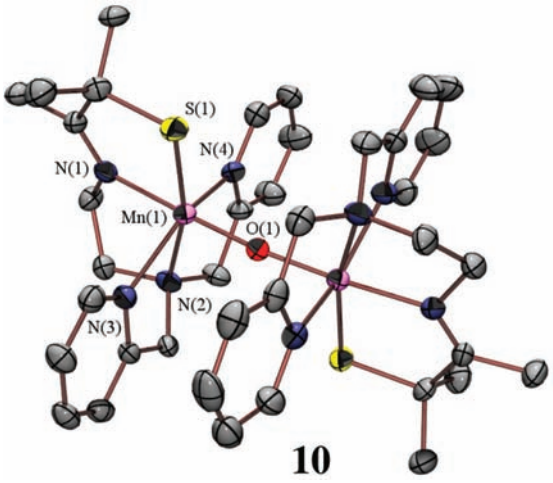

Figure 6. ORTEP diagram of $\{[Mn^{III}(S^{Me2}N_4(6\text{-H-DPEN})]_2\text{-}(\mu\text{-O})\}^{2+}$ (**10**) with counterions, solvents of crystallization, and hydrogen atoms omitted.

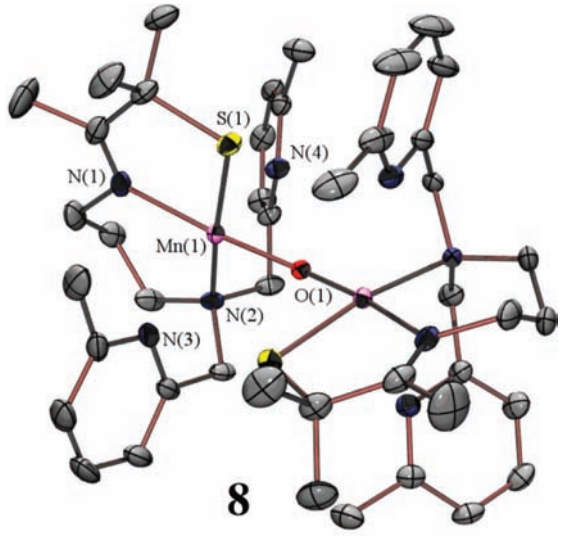

Figure 7. ORTEP diagram of $\{[Mn^{III}(S^{Me2}N_4(6\text{-Me-DPPN})]_2\text{-}(\mu\text{-O})\}^{2+}$ (**10**) with counterions, solvents of crystallization, and hydrogen atoms omitted.

plexes.[53−56] The instability of dimers **8** (Figure 7) and **9** (Supporting Information, Figure S-38) precluded a quantitative determination of the amount of O_2 necessary to form these species. Iodosylbenzene (PhIO, 0.5 equiv) addition to **1**, **2**, and **5** also affords dimers **6**, **7**, and **10**, respectively, in high yields at ambient temperatures, suggesting that a high-valent Mn(IV)═O intermediate forms along the O_2 reaction pathway.

Oxo-bridged dimer formation is readily monitored by electronic absorption spectroscopy, where, as shown in Figure 8 for thiolate-ligated **1**, O_2 addition results in the appearance of a broad, low-intensity band in the visible region, and a color change from pale yellow to a more intense purple. Electrospray mass spectral data shows that the bridging oxo atom in complexes **6**, **7**, and **10** is derived from $^{18}O_2$ (Supporting Information, Figures S-31−S-34). This, coupled with the fact that **6**−**10** were also shown to form via PhIO addition to **1**−**5**, implies that the mechanism of μ-oxo dimer formation involves O−O bond cleavage, via a metastable high-valent metal oxo intermediate. Metastable intermediates are detected in the low temperature (−40 °C) reaction between **1** and **2** and O_2 by electronic absorption spectroscopy and stopped-flow. The properties of these intermediates and the kinetics of their formation are currently being investigated, and will be discussed in a future manuscript. In contrast to **1** and **2**, intermediates are not observed in the low temperature reaction between complexes **3**−**5** and O_2, even at temperatures as low as −100 °C.

Structural and Magnetic Properties of Oxo-Bridged 6, 7, 8, and 10. Although there are numerous examples of μ-carboxylate-μ-oxo and bis-oxo Mn(III) dimers,[59−67] there are significantly fewer examples containing a single, unsupported oxo bridge.[57,58] The few reported examples display nearly linear Mn−O−Mn bridging angles, Mn···Mn separations of 3.4−3.6 Å, and six-coordinate Mn ions.[57,58] None of these examples include thiolate ligands. Solid-state magnetic susceptibility (χ_M) vs temperature data for **6**, **7**, and **10** were fit using julX[70] to the exchange Hamiltonian $\hat{H} = -2J(\hat{S}_1 \cdot \hat{S}_2)$ (where $S_1 = S_2 = 2$ and g

dx.doi.org/10.1021/ic300192q | Inorg. Chem. 2012, 51, 6633−6644

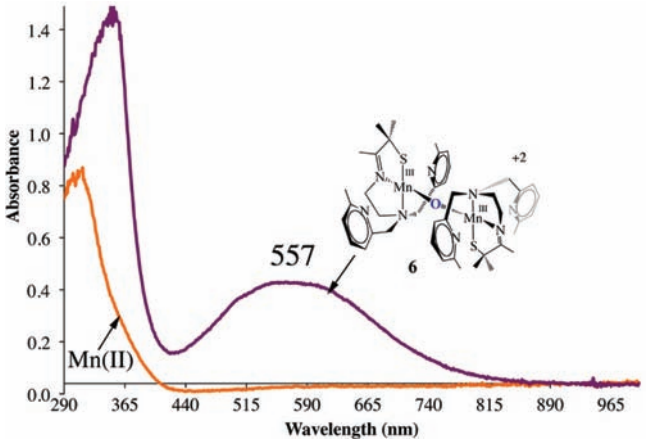

Figure 8. Electronic absorption spectra of $[Mn^{II}(S^{Me2}N_4(6\text{-Me-DPEN}))](BF_4)$ (**1**) (orange) and $[Mn^{III}(S^{Me2}N_4(6\text{-Me-DPEN})]_2\text{-}(\mu\text{-O})(BF_4)_2\cdot 2MeOH$ (**6**) (blue) in MeCN at room temperature.

~ 2) over the temperature range 5−300 K to afford *J*-values of $-125.6\ cm^{-1}$ (**6**), $-1.0\ cm^{-1}$ (**7**), and $-48.0\ cm^{-1}$ (**10**), which fall within the range seen with the few reported examples unsupported μ-oxo bridged Mn(III) dimers.[58,59] There does not appear to be any obvious correlation between the magnitude of this antiferromagnetic coupling constant and any particular metrical parameter for the series of dimers reported herein.

The Mn−S(1) bond lengths decrease by ~0.1 Å (Table 2) upon conversion of **1**−**5** to **6**−**10**, consistent with an increase in oxidation state from Mn(II) to Mn(III). The Mn(III)-SR bond lengths of **6**−**10** are comparable to those of five-coordinate Mn(III)-S(thiosalicylate) (2.2913(24) and 2.2752(25) Å),[68] but are notably shorter than those of dinuclear $[Mn_2(edt)_4]^{2-}$ (Mn(III)-RS_b = 2.632(2), Mn(III)-RS_t= 2.32 Å; RS_b = bridging, RS_t = terminal).[50] The oxo-bridging ligand of complexes **6**−**10** is *trans* to an imine nitrogen (Figures 5−7 and Supporting Information, Figure S-38), and the Mn−O−Mn bond angles vary from 180.0° in **6** to 146.15(11)° in **8**. The latter is, to our knowledge, the most acute bridging angle for an unsupported μ-oxo Mn(III) dimer, and is likely a consequence of steric congestion. Given that a more acute bridging angle would preclude the formation of strong, stabilizing π bonds between the oxo ligand and the Mn ions, the highly bent Mn−O−Mn angle in **8** is likely responsible for its instability. Complex **8** is also distinguished from the other dimers in terms of the relative orientation of the two halves of the dimer. In **6**, **7**, **9**, and **10** each half is rotated ~180° relative to one another, as shown by the relative positioning of the sulfurs (Figures 5−6), and the dihedral angle formed between the Mn(1)−S(1)−N(1)−N(2)−O(1) and Mn(1′)−S(1′)−N(1′)−N(2′)−O(1) planes (0°, 16.0°, 18.5°, and 7.1° for **6**, **7**, **9**, and **10**, respectively; Supporting Information, Figures S-43−S-46). In complex **8**, on the other hand, the Mn(1)−S(1)−N(1)−N(2)−O(1) and Mn(1′)−S(1′)−N(1′)−N(2′)−O(1) planes are nearly orthogonal 73.7° (Figure 7).

Another structural feature that perhaps contributes to the instability of dimeric **8** is the extrusion of one of the 6-methylpyridine moieties, in each half of the dimer, to a distance of 2.796 Å from the manganese center (Table 2, Figure 7). In contrast to what one would expect, all of the other Mn−N distances elongate (by nearly 0.5 Å) upon oxidation of Mn(II)-containing **1**−**3** to Mn(III)-containing **6**−**8** (Table 2). An increase in coordination number could account for some of the observed elongation, but typically this effect is not as pronounced as the metal ion radius decrease caused by oxidation. More likely an electronic stabilization gained upon distortion (akin to the Jahn−Teller effect, which strictly only applies to systems possessing O_h symmetry) provides a driving force for the elongation of trans $M\cdots N^{py,quin}$ bonds. The Mn−N(3) and Mn−N(4) distances for **6** and **7** are each significantly longer than the sum of both the Shannon covalent and ionic radii for a Mn(III)-N bond (2.105 Å),[44] suggesting that these two dimers are most accurately described as containing four-coordinate Mn(III) ions. The metrical parameters of **6** and **7** are overall relatively similar to one another and suggest that replacement of the 6-methylpyridine moieties in **6** with quinoline moieties in **7** only introduces minor structural perturbations. Sterics also appear to play a role in the trans $M\cdots N^{py,quin}$ bond elongation, given that the less sterically congested, unsubstituted (R= H) pyridine derivative **10** (Figure 6) does not have elongated Mn−N^{py} bonds (Table 2). This is further supported by comparing the bond lengths of **10** with those of $[Mn^{III}(S^{Me2}N_4(4\text{-MeO-3,5-Me}_2\text{-DPEN})]_2\text{-}(\mu\text{-O})(PF_6)_2\cdot 2MeCN$ (**11**).[69] Complex **11** (Figure 9) contains

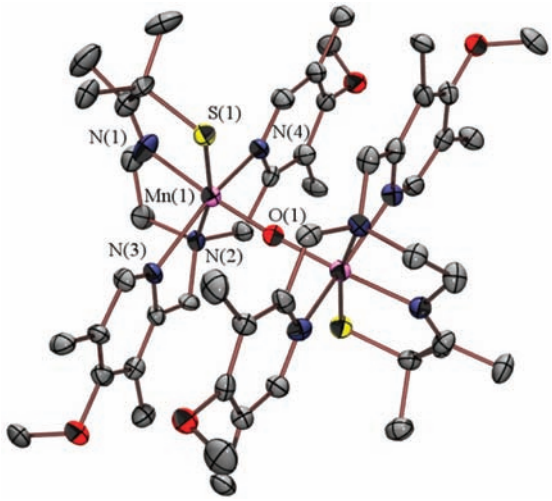

Figure 9. ORTEP diagram of $\{[Mn^{III}(S^{Me2}N_4(4\text{-MeO-3,5-Me}_2\text{-DPEN})]_2\text{-}(\mu\text{-O})\}^{2+}$ (**11**) with counterions, solvents of crystallization, and hydrogen atoms omitted. Selected distances (Å) and angles (degrees): Mn−$O(1)_{ave}$, 1.75(1); Mn−$S(1)_{ave}$, 2.28(2); Mn−$N(1)_{ave}$, 2.01(4); Mn−$N(2)_{ave}$, 2.18(2); Mn−$N(3,4)_{ave}$, 2.23(2); Mn−O(1)−Mn, 175.4(7).

substituents in the 3-, 4-, and 5-positions of the pyridine rings, but not in the 6-position, and the Mn−N(3) (2.219 Å) and Mn−N(4) (2.248 Å) bond distances are significantly shorter than those in the more sterically encumbered **6** (Figure 5; R(6-position) = Me) or **7** (Figure 5; R(6-position) = fused aryl), but comparable to those in less sterically encumbered **10** (R(6-position) = H). This demonstrates that the coordination geometry and metrics are particularly sensitive to bulky substituents in the 6-position of the pyridine ring. Noticeable differences in redox potentials provide additional evidence to support a higher coordination number in the less sterically congested Mn(III) dimer **10** (R = H) in the solution state, relative to the more bulky Mn(III) dimers **6** and **7**. The redox potential of **10** (+295 mV vs SCE) is significantly lower than all

dx.doi.org/10.1021/ic300192q | *Inorg. Chem.* 2012, 51, 6633−6644

of the other complexes reported herein, including **6** ($E_{1/2}$= +465 mV) and **7** (+780 mV (irrev). This drop in potential with **10** reflects an increase in electron density at the metal resulting from the higher coordination number (six). The higher coordination number appears to be facilitated by the less sterically encumbering (R = H) substituent.

Summary and Conclusions. We have synthesized and characterized a new series of five-coordinate, thiolate-ligated Mn(II) complexes with N-heterocylic-ligand scaffolds, and showed that each complex contains high-spin (S = 5/2) Mn(II) which is readily oxidized to the +3 oxidation state at modest potentials. Metrical parameters and geometric structure were found to be sensitive to minor structural changes, including the insertion of a methylene spacer and site-specific substitution of the N-heterocyclic moieties. The placement of substituents in the pyridine 6-position was shown to influence the ability of exogenous ligands to access and bind to the metal center, and insertion of a methylene unit was shown to alter the geometry from ∼trigonal bipyramidal to ∼square pyramidal. Each complex was shown to form a rare example of unsupported oxo-bridged Mn(III) dimer upon reaction with O_2. The more sterically congested 6-methylpyridine- and quinoline-ligated complexes were shown have unusually long Mn(III)-N-(pyridine) or Mn(III)-N(quinolone) distances, rendering these dimers coordinatively unsaturated. This effect is most pronounced when in addition to a 6-Me-pyridine substituent a methylene unit is inserted, causing both the 6-methylpyridine moiety to extrude itself from the metal ion's coordination sphere (Mn−N = 2.796) and the Mn−O−Mn bridging angle to become remarkably acute (146.15(11)°). This is in contrast to structures containing less congested unsubstituted pyridine rings where the metal ion was shown to be coordinatively saturated with significantly shorter Mn−N bonds. The Mn(III) ions in the reported oxo-bridged dimers were shown to be antiferromagnetically coupled with J-values in the range observed for the few reported examples of dimers containing an unsupported oxo-bridge.

■ ASSOCIATED CONTENT

Supporting Information

NMR and mass spec data for ligands L_1−L_5. Magnetic, electrochemical, and electronic absorption data for complexes **1**, **3**−**10**. Crystallographic tables for **1**, **3**−**10**. This material is available free of charge via the Internet at http://pubs.acs.org.

■ AUTHOR INFORMATION

Corresponding Author

*Phone: (206)543-0713. Fax: (206)685-8665. E-mail: kovacs@chem.washington.edu.

Notes

The authors declare no competing financial interest.

[†]UW Staff Crystallographers.

[‡]University of Nevada, Reno.

■ ACKNOWLEDGMENTS

NIH funding (#RO1GM45881-19) is gratefully acknowledged.

■ REFERENCES

(1) Oliw, E. H.; Jerneren, F.; Hoffmann, I.; Sahlin, M.; Garscha, U. *Biochim. Biophys. Acta* **2011**, *1811*, 138−147.

(2) Hamberg, M.; Su, C.; Oliw, E. *J. Biol. Chem.* **1998**, *273*, 13080−13088.

(3) Su, C.; Sahlin, M.; Oliw, E. H. *J. Biol. Chem.* **2000**, *275*, 18830−18835.

(4) Goldsmith, C. R.; Cole, A. P.; Stack, T. D. P. *J. Am. Chem. Soc.* **2005**, *127*, 9904−9912.

(5) Boal, A. K.; Cotruvo, J. A., Jr.; Stubbe, J.; Rosenzweig, A. C. *Science* **2010**, *329*, 1526−1530.

(6) Jackson, T. A.; Brunold, T. C. *Acc. Chem. Res.* **2004**, *37*, 461−470.

(7) Miller, A. F. *Acc. Chem. Res.* **2008**, *41*, 501−510.

(8) Vance, C. K.; Miller, A.-F. *Biochemistry* **2001**, *40*, 13079−13087.

(9) Bull, C.; Niederhoffer, E. C.; Yoshida, T.; Fee, J. A. *J. Am. Chem. Soc.* **1991**, *113*, 4069−4076.

(10) Wu, A. J.; Penner-Hahn, J. E.; Pecoraro, V. L. *Chem. Rev.* **2004**, *104*, 903−938.

(11) Umena, Y.; Kawakami, K.; Shen, J.-R.; Kamiya, N. *Nature* **2011**, *473*, 55−60.

(12) McEvoy, J. P.; Brudvig, G. W. *Chem. Rev.* **2006**, *106*, 4455−4483.

(13) Coggins, M. K.; Kovacs, J. A. *J. Am. Chem. Soc.* **2011**, *133*, 12470−12473.

(14) Shook, R. L.; Peterson, S. M.; Greaves, J.; Moore, C.; Rheingold, A. L.; Borovik, A. S. *J. Am. Chem. Soc.* **2011**, *133*, 5810−5817.

(15) Fukuzumi, S.; Kotani, H.; Prokop, K. A.; Goldberg, D. P. *J. Am. Chem. Soc.* **2011**, *133*, 1859−1869.

(16) Shook, R. L.; Gunderson, W. A.; Greaves, J.; Ziller, J. W.; Hendrich, M. P.; Borovik, A. S. *J. Am. Chem. Soc.* **2008**, *130*, 8888.

(17) Jin, N.; Ibrahim, M.; Spiro, T. G.; Groves, J. T. *J. Am. Chem. Soc.* **2007**, *129*, 12416−12417.

(18) Jin, N.; Lahaye, D. E.; Groves, J. T. *Inorg. Chem.* **2010**, *49*, 11516−11524.

(19) Bossek, U.; Weyhermuller, T.; Wieghardt, K.; Nuber, B.; Weiss, J. *J. Am. Chem. Soc.* **1990**, *112*, 6387−6388.

(20) VanAtta, R. B.; Strouse, C. E.; Hanson, L. K.; Valentine, J. S. *J. Am. Chem. Soc.* **1987**, *109*, 1425−1434.

(21) Geiger, R. A.; Chattopadhyay, S.; Day, V. W.; Jackson, T. A. *J. Am. Chem. Soc.* **2010**, *132*, 2821−2831.

(22) Annaraj, J.; Cho, J.; Lee, Y.-M.; Kim, S. Y.; Latifi, R.; de Visser, S. P.; Nam, W. *Angew. Chem., Int. Ed.* **2009**, *48*, 4150−4153.

(23) Seo, M. S.; Kim, J. Y.; Annaraj, J.; Kim, Y.; Lee, Y.-M.; Kim, S.-J.; Nam, W. *Angew. Chem., Int. Ed.* **2007**, *46*, 377−380.

(24) Lansky, D. E.; Goldberg, D. P. *Inorg. Chem.* **2006**, *45*, 5119−5125.

(25) Kitajima, N.; Komatsuzaki, H.; Hikichi, S.; Osawa, M.; Moro-oka, Y. *J. Am. Chem. Soc.* **1994**, *116*, 11596−11597.

(26) Groves, J. T.; Watanabe, Y.; McMurry, T. J. *J. Am. Chem. Soc.* **1983**, *105*, 4489−4490.

(27) Sono, M.; Roach, M. P.; Coulter, E. D.; Dawson, J. H. *Chem. Rev.* **1996**, *96*, 2841−2887.

(28) Denisov, I. G.; Makris, T. M.; Sligar, S. G.; Schlichting, I. *Chem. Rev.* **2005**, *105*, 2253−2277.

(29) Katona, G.; Carpentier, P.; Niviere, V.; Amara, P.; Adam, V.; Ohana, J.; Tsanov, N.; Bourgeois, D. *Science* **2007**, *316*, 449−453.

(30) Kovacs, J. A.; Brines, L. M. *Acc. Chem. Res.* **2007**, *40*, 501−509.

(31) Villar-Acevedo, G.; Nam, E.; Fitch, S.; Benedict, J.; Freudenthal, J.; Kaminsky, W.; Kovacs, J. A. *J. Am. Chem. Soc.* **2011**, *133*, 1419−1427.

(32) Sun, N.; Dey, A.; Villar-Acevedo, G.; Kovacs, J. A.; Darensbourg, M. Y.; Hodgson, K. O.; Hedman, B.; Solomon, E. *Inorg. Chem.* **2011**, *50*, 427−436.

(33) Swartz, R. D.; Coggins, M. K.; Kaminsky, W.; Kovacs, J. A. *J. Am. Chem. Soc.* **2011**, *133*, 3954−3963.

(34) Kitagawa, T.; Dey, A.; Lugo-Mas, P.; Benedict, J.; Kaminsky, W.; Solomon, E.; Kovacs, J. A. *J. Am. Chem. Soc.* **2006**, *128*, 14448−14449.

(35) Theisen, R. M.; Shearer, J.; Kaminsky, W.; Kovacs, J. A. *Inorg. Chem.* **2004**, *43*, 7682−7690.

(36) Nam, E.; Alokolaro, P. E.; Swartz, R. D.; Gleaves, M. C.; Pikul, J.; Kovacs, J. A. *Inorg. Chem.* **2011**, *50*, 1592−1602.

(37) Shearer, J.; Scarrow, R. C.; Kovacs, J. A. *J. Am. Chem. Soc.* **2002**, *124*, 11709−11717.

(38) Brines, L. M.; Villar-Acevedo, G.; Kitagawa, T.; Swartz, R. D.; Lugo-Mas, P.; Kaminsky, W.; Benedict, J. B.; Kovacs, J. A. *Inorg. Chim. Acta* **2008**, *361*, 1070−1078.
(39) Brines, L. M.; Shearer, J.; Fender, J. K.; Schweitzer, D.; Shoner, S. C.; Barnhart, D.; Kaminsky, W.; Lovell, S.; Kovacs, J. A. *Inorg. Chem.* **2007**, *46*, 9267−9277.
(40) Brown, C. D.; Neidig, M. L.; Neibergall, M. B.; Lipscomb, J. D.; Solomon, E. I. *J. Am. Chem. Soc.* **2007**, *129*, 7427−7438.
(41) Green, M. T.; Dawson, J. H.; Gray, H. B. *Science* **2004**, *304*, 1653−1656.
(42) Evans, D. A. *J. Am. Chem. Soc.* **1959**, 2005.
(43) Van Geet, A. L. *Anal. Chem.* **1968**, *40*, 2227−2229.
(44) Shannon, R. D. *Acta Crystallogr.* **1976**, *32*, 751−767.
(45) Hayashi, T.; Kayatami, T.; Sugimoto, H.; Suzuki, M.; Inomata, K.; Uehara, A.; Mizutani, T.; Kitagawa, T.; Maeda, Y. *J. Am. Chem. Soc.* **1995**, *117*, 11220−11229.
(46) Zang, Y.; Kim, J.; Dong, Y.; Wilkinson, E. C.; Appelman, E. H.; Que, L., Jr. *J. Am. Chem. Soc.* **1997**, *119*, 4197−4205.
(47) Maiti, D.; Woertink, J. S.; Narducci Sarjeant, A. A.; Solomon, E. I.; Karlin, K. D. *Inorg. Chem.* **2008**, *47*, 3787−3800.
(48) Addison, A. W.; Rao, T. N.; Reedijk, J. *J. Chem. Soc., Dalton Trans.* **1984**, 1349−1356 ; τ is defined as $(a - b)/60$, where a = largest angle, b = second largest angle (τ = 1.0 for ideal trigonal bipyramidal; τ = 0.0 for ideal square pyramidal).
(49) Schweitzer, D.; Shearer, J.; Rittenberg, D. K.; Shoner, S. C.; Ellison, J. J.; Loloee, R.; Lovell, S.; Barnhart, D.; Kovacs, J. A. *Inorg. Chem.* **2002**, *41*, 3128−3136.
(50) Costa, T.; Dorfman, J. R.; Hagen, K. S.; Holm, R. H. *Inorg. Chem.* **1983**, *22*, 4091−4099.
(51) Matsunaga, Y.; Fujisawa, K.; Ibi, N.; Miyashita, Y.; Okamoto, K.-I. *Inorg. Chem.* **2005**, *44*, 325−335.
(52) Gorelsky, S. I.; Basumallick, L.; Vura-Weis, J.; Sarangi, R.; Hodgson, K. O.; Hedman, B.; Fujisawa, K.; Solomon, E. I. *Inorg. Chem.* **2005**, *44*, 4947−4960.
(53) Grapperhaus, C. A.; Darensbourg, M. Y. *Acc. Chem. Res.* **1998**, *31*, 451−459.
(54) Lugo-Mas, P.; Dey, A.; Xu, L.; Davin, S. D.; Benedict, J.; Kaminsky, W.; Hodgson, K. O.; Hedman, B.; Solomon, E. I.; Kovacs, J. A. *J. Am. Chem. Soc.* **2006**, *128*, 11211.
(55) Liu, T.; Li, B.; Singleton, M. L.; Hall, M. B.; Darensbourg, M. Y. *J. Am. Chem. Soc.* **2009**, *131*, 8296−8307.
(56) Jiang, Y.; Widger, L. R.; Kasper, G. D.; Siegler, M. A.; Goldberg, D. P. *J. Am. Chem. Soc.* **2010**, *132*, 12214−12215.
(57) Badiei, Y. M.; Siegler, M. A.; Goldberg, D. P. *J. Am. Chem. Soc.* **2011**, *133*, 1274−1277.
(58) Mukhopadhyay, S.; Mandal, S. K.; Bhaduri, S.; Armstrong, W. H. *Chem. Rev.* **2004**, *104*, 3981−4026.
(59) Mullins, C. S.; Pecoraro, V. L. *Coord. Chem. Rev.* **2008**, *252*, 416−443.
(60) Vogt, L. H., Jr.; Zalkin, A.; Templeton, D. H. *Science* **1966**, *151*, 569−570.
(61) Vogt, L. H., Jr.; Zalkin, A.; Templeton, D. H. *Inorg. Chem.* **1967**, *6*, 1725−1730.
(62) Ziolo, R. F.; Stanford, R. H.; Rossman, G. R.; Gray, H. B. *J. Am. Chem. Soc.* **1974**, *96*, 7910−7915.
(63) Kipke, C. A.; Scott, M. J.; Gohdes, J. W.; Armstrong, W. H. *Inorg. Chem.* **1990**, *29*, 2193−2194.
(64) Horner, O.; Anxolabéhère-Mallart, E.; Charlot, M.-F.; Tchertanov, L.; Guilhem, J.; Mattioli, T. A.; Boussac, A.; Girerd, J.-J. *Inorg. Chem.* **1999**, *38*, 1222−1232.
(65) Baffert, C.; Collomb, M.-N.; Deronzier, A.; Pécaut, J.; Limburg, J.; Crabtree, R. H.; Brudvig, G. W. *Inorg. Chem.* **2002**, *41*, 1404−1411.
(66) Triller, M. U.; Hsieh, W.-Y.; Pecoraro, V. L.; Rompel, A.; Krebs, B. *Inorg. Chem.* **2002**, *41*, 5544−5554.
(67) Ghosh, K.; Eroy-Reveles, A. A.; Olmstead, M. M.; Mascharak, P. K. *Inorg. Chem.* **2005**, *44*, 8469−8475.
(68) Seela, J. L.; Knapp, M. J.; Kolack, K. S.; Chang, H.-R.; Huffman, J. C.; Hendrickson, D. N.; Christou, G. *Inorg. Chem.* **1998**, *37*, 516−525.
(69) We were unsuccessful at obtaining clean samples of the reduced mononuclear precursor to **11**, $[Mn^{II}(S^{Me2}N_4(4\text{-MeO-}3,5\text{-}Me_2\text{-DPEN})]^+$, despite numerous attempts. Aerobic oxidation of crude mixtures presumably containing this reduced species resulted in an intractable mixture of compounds. However, we were able to successfully obtain a few very small crystals of **11** that were suitable for X-ray diffraction studies.
(70) http://ewww.mpi-muelheim.mpg.de/bac/logins/bill/julX_en.php.